Iron clustering in GaSe epilayers grown on GaAs(111)B



2006 J. Phys.: Condens. Matter 18 1165

(http://iopscience.iop.org/0953-8984/18/4/005)

INSTITUTE OF PHYSICS PUBLISHING JOURNAL OF PHYSICS: CONDENSED MATTER

J. Phys.: Condens. Matter **18** (2006) 1165–1174 doi:10.1088/0953-8984/18/4/005

# Iron clustering in GaSe epilayers grown on GaAs(111)B

**A R de Moraes[1], D H Mosca[1], N Mattoso[1], J L Guimarães[1], J J Klein[1], W H Schreiner[1], P E N de Souza[2], A J A de Oliveira[2], M A Z de Vasconcellos[3], D Demaille[4], M Eddrief[4] and V H Etgens[4]**

[1] Departamento de Física, Universidade Federal do Paraná, 81531-990 Curitiba PR, Brazil
[2] Departamento de Física, Universidade Federal de São Carlos, 13565-905 São Carlos SR, Brazil
[3] Instituto de Física, Universidade Federal do Rio Grande do Sul, 91501-970 Porto Alegre RS, Brazil
[4] Institute de NanoScience de Paris, Université de Paris VI, 75252 Paris, France

Received 1 November 2005
Published 9 January 2006
Online at stacks.iop.org/JPhysCM/18/1165

**Abstract**

In this paper we report on the structural, morphological and magnetic properties of semiconducting GaSe epilayers, grown by molecular beam epitaxy, doped to different iron contents (ranging from 1 to 22 at.% Fe). Our results indicate that iron forms metallic Fe nanoparticles with diameters ranging from 1 to 20 nm embedded in the crystalline GaSe matrix. The Fe incorporation proceeds by segregation and agglomeration and induces a progressive disruption of the lamellar GaSe epilayers. The magnetization as a function of the temperature for zero-field cooling with the magnetic field parallel to the surface of the sample provides evidence of superparamagnetic behaviour of the nanoparticles. Cathodoluminescence experiments performed at room temperature reveal semiconducting behaviour even for samples with Fe concentrations as high as 20 at.%.

## 1. Introduction

Semiconductor-based magnetic materials such as ferromagnet/semiconductor and diluted magnetic semiconductors have generated much interest in research on spintronics due to the possibility of exploring the flexibility of carrier concentration and polarization of spin at room temperature [1, 2]. GaSe is a highly anisotropic semiconductor compound with a sequential stacking of sheets consisting of Se–Ga–Ga–Se atomic layers. Ionic–covalent forces bind the atoms within the elementary layers while van der Waals-like forces keep the layers together, since no dangling bonds are formed in the Se layers. Interest in GaSe is due largely to its non-linear optical properties, particularly for optical frequency conversion in the near- to mid-infrared [3]. Pekarek *et al* [4] have reported the fabrication of a diluted magnetic semiconductor by Mn doping of the GaSe compound, whereas Zerrouki [5] *et al* have reported

  

**Table 1.** Growth conditions used for the preparation of GaSe–Fe granular films on GaSe/GaAs(111)B substrates. Fe concentrations in the samples were estimated from the x-ray photoemission experiments.

| | GaSe–Fe | | |
|---|---|---|---|
| Sample | $T_{sub}$ (K) | $T_{Fe}$ (K) | Fe concentration (at.%) |
| a | 660 | 1673 | 7.0 |
| b | 655 | 1623 | 1.0 |
| c | 625 | 1653 | 7.0 |
| d | 625 | 1693 | 10.0 |
| e | 555 | 1703 | 20.0 |
| f | 475 | 1693 | — |
| g | 475 | 1653 | — |
| h | 555 | 1723 | 20.0 |
| i | 555 | 1673 | 7.0 |
| j | 650 | — | — |
| k | 650 | — | — |
| l | 623 | 1723 | 20.0 |
| m | 623 | 1723 | 22.0 |
| n | 650 | — | — |

the feasibility of a sequential growth of discontinuous Fe layers onto GaSe. The interesting optical response together with an exceptional chemical stability motivated us to investigate a novel GaSe-based material consisting of Fe and GaSe in a co-deposition regime forming iron nanoparticles embedded in GaSe. The structural, morphological and magnetic properties as well as the chemical stability of these hybrid metal–semiconductor nanostructures are described and discussed.

## 2. Experimental details

The growth of Fe epilayers on GaSe as well as GaSe-based epilayers with Fe incorporation using molecular beam epitaxy (MBE) in an ultrahigh vacuum system equipped with reflection high energy electron diffraction (RHEED) has been previously described by our group [6–8]. For the present study, GaAs(111)B substrates were used. After the oxide desorption, a very thin GaAs buffer layer was deposited. Next, a GaSe epilayer was deposited with a thickness of about 6 nm ($\sim 7\frac{1}{2}$ sheets), ensuring a complete structural relaxation [7, 9] of the misfit strain while also blocking interdiffusion between Fe and the GaAs substrate. The GaSe–Fe granular films were grown onto this first GaSe seed layer. The samples were grown at substrate temperatures ($T_{sub}$) between 470 and 660 K. Two different growth rates for GaSe were used, 1.1 and 0.55 nm min$^{-1}$, while maintaining the same Se/Ga partial pressure ratio fixed at 8:10 [7, 8]. The Fe concentration in the samples was controlled by changing the Fe source-cell temperature ($T_{Fe}$). The growth parameters that we consider relevant are shown in table 1. In summary, samples j and k were grown at a rate of 1.1 nm min$^{-1}$, whereas samples m and n were grown at 0.55 nm min$^{-1}$, with sample n being a simple GaSe buffer layer. To perform *ex situ* experiments, a 10 nm thick capping layer of amorphous ZnSe was deposited in order to protect the structure against air exposure.

XPS experiments were performed using Mg K$\alpha$ radiation ($h\nu = 1253.6$ eV) with an overall energy resolution of 0.8 eV. *Ex situ* XPS was carried out using a VG Microtech

(ESCA3000) commercial system with a base pressure of $3 \times 10^{-10}$ mbar and a hemispherical energy analyser positioned at 45° to the sample surface normal. XPS profiles were obtained using argon ion bombardment (3 kV, 5 $\mu$A) that corresponds to a sputter rate of about 0.2 nm min$^{-1}$ for the ZnSe capping layer. Analytical software (VGX900-W) available in the equipment was used to estimate the surface stoichiometry taking into account atomic sensitivities. XPS analyses were used to determine the surface stoichiometry of the samples as a function of the thickness and iron content (which ranged in between 1 and 22 at.%). X-ray diffraction (XRD) measurements were performed at room temperature using conventional $\theta$–$2\theta$ scans in a Bragg–Brentano geometry with Co radiation in order to minimize the contribution from fluorescence. Transmission electron microscopy (TEM) analyses including selected-area electron diffraction (SAED) were performed using a transmission electron microscope (JEOL 1200EX-II) operating at 120 kV. Magnetic measurements were performed with a SQUID magnetometer (Quantum Design MPMS 5S) with temperature ranging between 10 and 300 K and magnetic field up to 10 kOe, oriented in the plane of the film. Zero-field-cooling (ZFC) and field-cooling (FC) magnetization curves were employed to study the magnetic behaviour of samples. Cathodoluminescence (CL) experiments were performed to characterize the electronic behaviour of the samples by employing an electron microprobe (Cameca SX50) equipped with a diffraction grating (SP500i monochromator/spectrometer) and CCD detector.

## 3. Analyses and discussion

### *3.1. Chemical analyses*

The samples were studied after preparation by x-ray photoemission spectroscopy (XPS). A mild ion-erosion of the heterostructure allows investigating the top-down composition by monitoring the XPS signals of the Ga, Se and Fe core levels. The XPS spectra of As 3d and Se 3d core levels with respect to reference GaAs and GaSe photoemission signals are consistent with a sharp interface between epilayer and substrate and with no visible signs of chemical reactivity between them.

XPS signals of the Ga, Se and Fe core levels are shown in figure 1 for samples m, a and i. The spectra were only corrected with respect to the energy shifts (about 2 eV) related to charge effects. These spectra illustrate the chemical state and stoichiometry of samples with different Fe concentrations (7 or 22 at.% Fe) or different substrate temperatures (from 555–660 K). The spectra were arbitrarily shifted vertically relative to each other to allow better visualization. XPS spectra for bulk Fe and bulk GaSe measured under the same conditions are also shown for comparison. No indication of intermediary compound formation can be found. Since the Fe concentration does not exhibit a dependence on $T_{sub}$, it was assumed that the sticking coefficient for the Fe atoms does not change in the temperature interval studied.

The amount of Fe incorporated in the films was calculated by means of the integrated area ratio of the *in situ* and *ex situ* XPS signals of the Fe 2p, Ga 2p and Se 3d spectra after background subtraction [10], corrected with the atomic sensitivities and cross sections. XPS experiments were used to estimate the average atomic concentrations of the samples with an instrumental resolution of 1 at.% and an accuracy of 12% of the nominal values. For example, XPS profiles (not shown) obtained after $Ar^+$ bombardment of the a and m samples indicate that the elemental concentration as a function of depth for sample a stabilizes at ∼7 at.% Fe, whereas for sample m it reaches ∼22 at.% Fe. Table 1 displays the growth conditions and the Fe concentration estimated from XPS experiments. As expected, the Fe concentration increases when $T_{Fe}$ increases, from ∼1 at.% for $T_{Fe} = 1623$ K to ∼22 at.% for $T_{Fe} = 1723$ K.

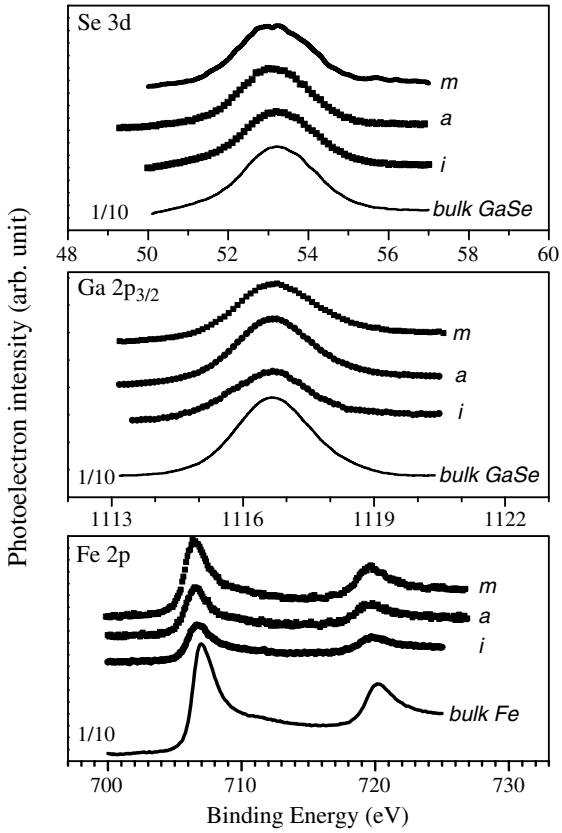


**Figure 1.** Typical *ex situ* XPS spectra of the Se 3d, Ga $2p_{3/2}$ and Fe $2p_{3/2-1/2}$ core levels for samples m, a and i deposited under conditions given in table 1. The spectra were collected after 30 min of Ar ion bombardment on the plateaus of the Fe concentrations. Plots of Se 3d, Ga $2p_{3/2}$ and Fe $2p_{3/2-1/2}$ core level spectra, respectively, appear at the bottom of each panel, as measured for bulk Fe and bulk GaSe samples.

It also increases when the GaSe growth rate is reduced from 1.1 to 0.55 nm $min^{-1}$ at higher values of $T_{Fe}$. For example, sample m ($T_{Fe} = 1723$ K) exhibits the highest Fe concentration.

### *3.2. Structural analyses*

Previous XRD experiments [6] indicated the presence of the complete family of atomic (00$n$) planes for $n = 3, 6, 9, \ldots, 21$, associated with the formation of the $\gamma$ polytype of GaSe having a lattice parameter $c = 7.9$ Å for samples grown at $T_{sub} > 550$ K. XRD patterns indicate the integrity of GaSe even when Fe incorporation reaches the highest Fe concentration; i.e., 22 at.% Fe.

A comparison between the (006) Bragg reflections for samples k and l grown at the same rate of 1.1 nm $min^{-1}$ and with similar substrate temperatures is shown in figure 2. The diffractograms were normalized with respect to the x-ray intensity of the GaAs(111) Bragg reflection for Co K$\beta$ radiation, which was used to optimize the alignment of the samples. Both the distinct normalized intensity and the profile shape clearly indicate the tendency towards structural degradation of the GaSe epilayer due to the Fe incorporation. The XRD pattern of the pure GaSe epilayer (sample k) exhibits thickness interference fringes as shown in the inset.

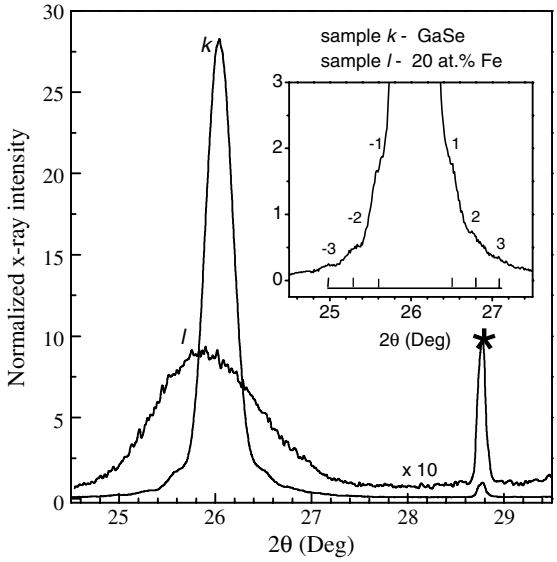


**Figure 2.** XRD patterns showing Bragg reflections corresponding to $\gamma$-GaSe(006) planes of samples k and l grown onto GaAs(111)B substrates at the same growth rate 1.1 nm min$^{-1}$ and similar substrate temperatures. The x-ray intensities are given in arbitrary units normalized with respect to the diffraction peak marked with an asterisk (*) which corresponds to the Bragg reflection of the GaAs(111) plane for Co K$\beta$ radiation. The inset shows a set of three thickness fringes in the x-ray profile of the GaSe epilayer.

These oscillations provide very direct evidence that the crystalline quality of the GaSe epilayer is rather high. The thickness value estimated from the position of the thickness fringes in the x-ray profile is in good agreement with nominal sample thickness; i.e., 55 nm.

According to XPS analyses, the Fe concentration in sample l is ∼20 at.% Fe. A rather significant reduction in the x-ray intensity is observed for this sample indicating that Fe content is a detrimental factor for the crystal. It clearly induces a degradation of the coherence length in the GaSe crystalline layered structure. GaSe integrity, however, is preserved along the growth direction. A slight shift of the Bragg reflection towards lower angular positions is observed for sample l compared to sample k, indicating that the average lamellar distance is expanded by approximately ∼0.63%. This expansion along the growth direction is probably associated with strain. However, Fe incorporation in the van der Waals gap of the GaSe layered structure cannot be discarded [5].

Therefore, the Fe incorporation in the films is detrimental to the stacking of the atomic planes of $Ga_2Se_2$ which growth mode involves terrace completion rather than a layer-by-layer overgrowth. The angular resolution and atomic sensitivity of these XRD experiments, however, do not allow their use for investigating the chemical state of Fe atoms or possible compound formation, between Fe and GaSe.

TEM analyses were performed to access the microstructure and micromorphology of the samples without an objective aperture to enhance the electronic density contrast. A TEM image in bright field of sample m is shown in figure 3(a). Dark regions with higher electronic density and irregular shapes are presumably isolated Fe particles dispersed in the GaSe host having a lamellar structure and lowest electronic contrast. By assuming that the particles with sizes varying from 2 to 16 nm (mean size $\langle d \rangle = 6$ nm) have spheroidal shapes, the corresponding volumes are estimated to be between 4 and 2000 nm$^3$. A careful inspection of the GaSe

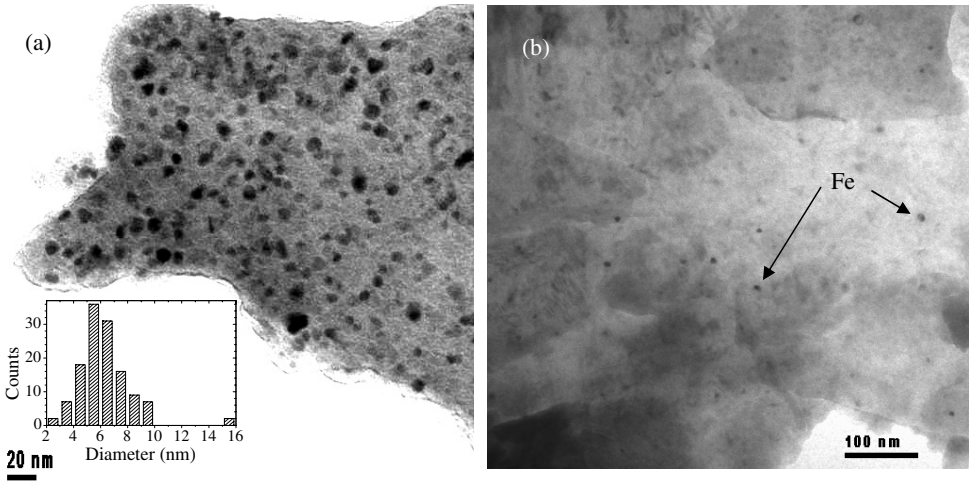


**Figure 3.** (a) Bright field TEM image for sample m with 22 at.% Fe. Dark regions visible inside the GaSe lamellar structure correspond to Fe nanoclusters. The particle size distribution of the TEM image is shown in the inset. (b) Bright field TEM image for sample b with 1 at.% Fe.

host reveals the presence of crystalline grains surrounding each Fe particle, indicating that Fe incorporation induces a disruption of the GaSe. The particle size distribution is shown in the inset of figure 3(a). The particles have an average diameter of about 6 nm corresponding to an average volume of 100 $nm^3$. A TEM image of sample b having the concentration of 1 at.% Fe is shown in figure 3(b). A reduced number of small Fe particles dispersed in the lamellar host can still be observed, despite the small Fe concentration.

Selected-area electron diffraction (not shown) indicates several diffraction spots associated with the Bragg reflections of some $\gamma$-GaSe grains. Therefore, the spotted character of the electron diffraction indicates a reduction of the lateral coherence suggesting that a mosaic GaSe crystal is formed when the Fe amount is increased in the samples.

### *3.3. Magnetic properties*

Magnetic moment measurements carried out with a SQUID magnetometer are shown in figure 4. Magnetization versus magnetic field ($M-H$) curves measured at 5 and 300 K for sample i are shown and details of the inner part of the loops are inserted at the lower right of the figure. For 5 K, a remanence ($M_r$) corresponding to 37.1% of the saturation magnetization value ($M_s$) with a coercive field ($H_c$) of about 250 Oe is observed. On increasing the temperature to 300 K, the $M_r$ value decreases to about 1.3% $M_s$, whereas $H_c$ becomes smaller than the magnetic field step (10 Oe in this measurement), indicating that hysteresis is almost entirely absent. This is consistent with the presence of small magnetic particles weakly interacting in a blocked state.

The magnetic behaviour of an assembly of small particles with a weak magnetic interaction between them going from a blocking state to a superparamagnetic state can be described by a Langevin function. Tentatively, $M-H$ curves were fitted by a Langevin function given by $M/M_s = \coth(\langle\mu\rangle H/k_BT) - (k_BT/\langle\mu\rangle H)$, where an average magnetic moment per particle ($\langle\mu\rangle$) is used. Since the magnetic moment of the particles is directly related to their volumes, the average magnetic moment can be written as $\langle\mu\rangle = M_s\langle V\rangle$, where $M_s = 1710$ emu $cm^{-3}$ is the saturation magnetization (assumed as the same value found for bulk Fe at 298 K [11]) and

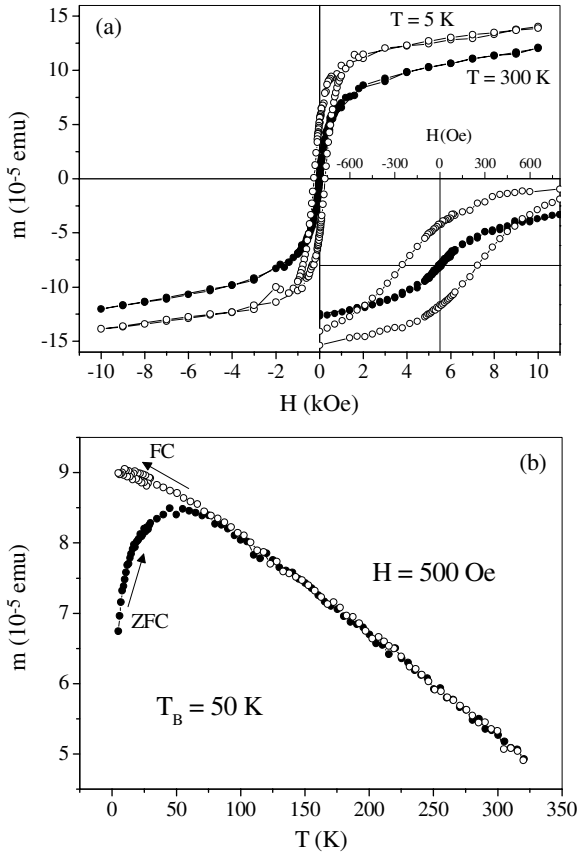


**Figure 4.** (a) Magnetic moment versus applied field curves for sample i. The inset, bottom right, shows the inner part of the magnetization loops. (b) ZFC and FC magnetic moment curves obtained for a field cooling of 500 Oe applied in the film plane.

$\langle V \rangle$ is a parameter of the fit corresponding to an average magnetic volume per particle. The magnetic behaviour of the samples can also include a small and negative slope associated with a diamagnetic response of the GaSe seed layer and GaAs substrate. A constant ferromagnetic response was also superimposed on the superparamagnetism due to either the possible presence of particles having sizes larger than 20 nm (critical size for Fe monodomains) or interactions among small particles close enough to promote an effective magnetic coupling leading to cluster ferromagnetism. The $M-H$ curves measured at room temperature were fitted by a Langevin function after subtracting the diamagnetic slope of GaAs and the almost negligible ferromagnetic constant.

Table 2 displays the values of $\langle \mu \rangle$ and average volume $\langle V \rangle$ obtained from the Langevin fitting of the $M-H$ curves of the samples. The average magnetic volume per particle obtained as a fitting parameter for sample m is $\langle V \rangle = 100\ \text{nm}^3$. This value is in good agreement with the most probable volume of the particles obtained from the statistical analyses of the particle size distribution adopting spheroidal shapes, as shown in the inset of figure 3(a). According to table 2, the average magnetic moment per particle does not exhibit a direct correlation with the Fe concentration. As can be seen, the substrate temperature together with Fe and GaSe growth rates has a strong influence on the average magnetic moment per particle in the superparamagnetic state.

**Table 2.** Some magnetic data as obtained from the SQUID magnetometry. The values of $\langle m \rangle$ and $V$ were obtained form the Langevin fitting of the magnetization versus field curves, whereas $T_B$ corresponds to a maximum in the ZFC magnetization curves.

| Sample | Fe concentration (at.%) | $\langle \mu \rangle$ ($10^{-16}$ emu) | $\langle V \rangle$ ($nm^3$) | $T_B$ (K) |
|---|---|---|---|---|
| a | 7.0 | 1.2 | 70 | 137 |
| i | 7.0 | 2.0 | 117 | 50 |
| d | 10.0 | — | — | |
| e | 20.0 | 1.1 | 64 | 160 |
| l | 20.0 | 4.5 | 263 | 110 |
| m | 22.0 | 1.7 | 100 | — |

The presence of an assembly of magnetic particles with a broad size distribution is corroborated by zero-field-cooling (ZFC) and field-cooling (FC) magnetization curves. Typical ZFC and FC curves are shown in the inset upper left in figure 4. The magnetic irreversibility associated with a branching between ZFC and FC curves, and a peak in the ZFC curve corresponding to a blocking temperature ($T_B$) are two strong indications of superparamagnetism consistent with the presence of magnetic Fe nanoparticles. $T_B$ values of selected samples are given in the table 2. Again, it is difficult to extract a correlation between $T_B$ values and Fe concentration. This is not surprising because the blocking temperature depends on the particle volumes already mentioned.

If the blocking temperature defined as $T_B = K\langle V \rangle / 25 k_B$ is used to obtain an effective anisotropy energy density with data shown in table 2, the calculated $K$ values range between $0.9 \times 10^5$ and $8.6 \times 10^5$ J m$^{-3}$. Thus, the anisotropy constant values, as a parameter obtained from the $M-H$ fit and ZFC magnetization, are between 2 and 20 times higher than the corresponding bulk value ($K_{Fe} = 0.5 \times 10^5$ J m$^{-3}$). Usually, the effective anisotropy values in granular systems are larger than bulk values for $K$ (which take into account only the magnetocrystalline contribution) because contributions from surface and magnetoelastic anisotropies could become important, as well as varying with the volume of the particles [12]. Therefore, caution is always necessary when estimating particle size directly from $T_B$.

We summarize the magnetic response of the incorporation of Fe in the GaSe epilayers as follows. SQUID measurements together with TEM and XPS analyses allow us to conclude that iron tends to cluster and form isolated Fe nanoclusters in the GaSe epilayers. At low temperature, the magnetization curves in all films, irrespective of Fe concentration, have a small remanence and an approach to saturation that is characteristic of randomly oriented particles with uniaxial anisotropy. Fe nanoparticles exhibit a superparamagnetic behaviour at room temperature with no significant magnetic interaction.

### *3.4. Cathodoluminescence*

The cathodoluminescence (CL) experiments have been performed at room temperature for samples displaying different Fe contents (figure 5). The CL spectra are characterized by one broad and intense band that is mainly located in the near infrared region. This is interpreted as an excitation of electrons into the conduction band followed by luminescent emission. The presence of an energy band gap of about $E_G = 1.8$ eV [13] is observed for all samples, suggesting a perfect semiconducting behaviour such as expected for bulk GaSe. The CL signals increase as a function of the increase of the Fe content and substrate temperature, as suggested by a comparison between samples with 7 at.% Fe. Sample h, having the highest Fe concentration (20 at.% Fe) in this set of samples, exhibits an attenuation in the CL signal which is probably associated with a strong structural disorder and defect density. However, even this

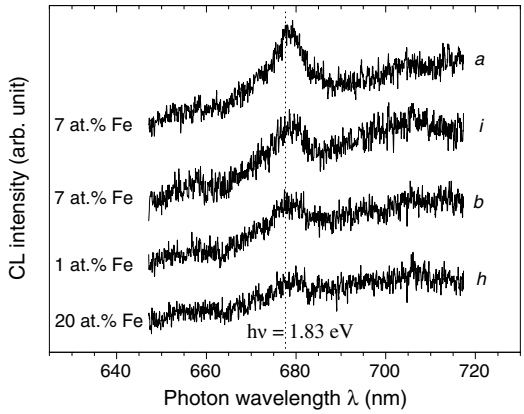


**Figure 5.** CL spectra measured at room temperature for a selected set of samples. The dashed line indicates the energy position corresponding to the band gap of the samples which is in quite good agreement with the band gap value expected for bulk GaSe.

sample still displays preservation of the GaSe band gap and semiconducting behaviour at room temperature.

## 4. Final remarks

Structural, morphological and magnetic properties of GaSe epilayers grown by MBE with different iron contents show that iron forms an assembly of metallic nanoparticles embedded in GaSe matrix grown on GaAs(111)B substrates. Fe nanoparticles exhibit a superparamagnetic behaviour at room temperature with no significant magnetic interaction. According to XRD and TEM analyses a strong structural disorder caused by GaSe lamellar disruption is progressively observed on increasing the Fe incorporation. Furthermore, the incorporation of Fe proceeds by segregation and agglomeration. According to x-ray diffraction, the integrity of GaSe along the growth direction persists even for concentrations as high as 22 at.% Fe. However, Fe clustering only reduces the lateral coherence of GaSe, without evidence of Fe insertion as a dopant in the $Ga_2Se_2$ sheets. Since GaSe growth proceeds predominantly in a layer-by-layer fashion with completion of consecutive $Ga_2Se_2$ sheets and not atomic plane by atomic plane, the increase of defects in the surroundings of the Fe clusters is probably due to deformation in the crystal grains by slip processes between lamellar sheets. This simple description is corroborated by experimental evidence of the capability of the layered structure to accommodate the strong lattice mismatches. Therefore, it is not surprising at all that a semiconducting behaviour at room temperature was preserved in a GaSe mosaic crystal even for heavy incorporation of Fe as indicated by cathodoluminescence.

To summarize, the GaSe–Fe granular films exhibit crystalline structure with the normal equilibrium $\gamma$ phase of GaSe with close packed planes parallel to the film surface. These samples could be used as interlayers for semiconductor/ferromagnetic metal heterostructures, or as novel magnetic material.

## Acknowledgments

The authors would like to thank CNPq, CAPES/Cofecub and FAPESP (grant 03/02804-8) for financial support. One of us (ARM) acknowledges the Brazilian agency CNPq for financial support.

## References


[1] Wolf S A, Awschalom D D, Buhrman R A, Daughton J M, von Molnar S, Roukes M L, Chtchelkanova A Y and Treger D M 2001 *Science* **294** 1488

[2] Malajovich I, Berry J J, Samarth N and Awschalom D D 2001 *Nature* **411** 770

[3] Singh N B, Suhre D R, Balakrishna V, Marable M, Meyer R, Fernelius N C, Hopkins F K and Zelmon D 1998 *Prog. Cryst. Growth Charact.* **37** 47

[4] Pekarek T M, Fuller C L, Garner J, Crooker B C, Miotkwski J and Ramdas A K 2001 *J. Appl. Phys.* **89** 7030

[5] Zerrouki M, Lacharme J P, Ghamnia M, Sebenne C A, Eddrief M and Abidri B 2000 *Appl. Surf. Sci.* **166** 143

[6] de Moraes A R, Mosca D H, Schereiner W H, Guimarães J L, de Oliveira A J A, de Souza P E N, Etgens V H and Eddrief M 2004 *J. Magn. Magn. Mater.* **272–276** 1551

[7] Eddrief M *et al* 2001 *Phys. Rev.* B **63** 094428

[8] Jedrecy N, Pinchaux R and Eddrief M 1997 *Phys. Rev.* B **56** 9583

[9] Koëbel A, Zheng Y, Petroff J F, Boulliard J C, Capelle B and Eddrief M 1997 *Phys. Rev.* B **56** 12296

[10] Moulder J F, Stickle W F, Sobol P E and Bomben K D 1995 *Handbook of X-ray Photoelectron Spectroscopy* (Minnesota, USA: Physical Electronics Inc) p 252

[11] Swartzendruber L J *et al* 1991 *J. Magn. Magn. Mater.* **100** 573

[12] Torres J M, Luis F, Garcia L M, Bartolome J, Stankiewicz J, Petroff F, Fettar F and Vaures A 2002 *J. Magn. Magn.* **242–245** 575

[13] Ohyama M and Fujita Y 2003 *Surf. Coat. Technol.* **169/170** 620